Revision 2

The 2*H* and 3*R* polytypes of sabieite, $NH_4Fe^{3+}(SO_4)_2$, from a natural fire in an oil-bearing shale near Milan, Ohio

ANTHONY R. KAMPF*[1], R. PETER RICHARDS[2] AND BARBARA P. NASH[3]

[1]Mineral Sciences Department, Natural History Museum of Los Angeles County, 900 Exposition Boulevard, Los Angeles, CA 90007, U.S.A.
[2]Geology Department, Oberlin College, Oberlin, OH 44074, U.S.A.
[3]Department of Geology and Geophysics, University of Utah, Salt Lake City, Utah 84112, U.S.A.
*Email: akampf@nhm.org

ABSTRACT

The mineral sabieite, $NH_4Fe^{3+}(SO_4)_2$, was found in 2011 along the banks of the Huron River near Milan, Ohio, where it formed as the result of a natural fire in an oil-bearing shale. The mineral is directly associated with pyracmonite, tschermigite and voltaite and occurs as colorless, pale pink, tan and yellow hexagonal tablets. The streak is white. Crystals are transparent with vitreous luster. Mohs hardness is 2½, tenacity is brittle, fracture is irregular and cleavage is perfect on {001}. The measured density is 2.65(2) $g \cdot cm^{-3}$. The mineral is optically uniaxial (–) with indices of refraction $\omega = 1.657(3)$ and $\varepsilon = 1.621(5)$ (white light). The empirical formula (based on 2 S *apfu*) is

$[(NH_4)_{0.73}(H_3O)_{0.22}K_{0.04}Na_{0.01}]_{\Sigma 1.00}(Fe^{3+}_{0.95}Al_{0.02}Mg_{0.01})_{\Sigma 0.98}(SO_4)_2$. Powder diffraction showed crystals to be combinations of the 2*H* and 3*R* polytypes. The structure of the 2*H* polytype was solved and refined from single-crystal data yielding $R_1 = 0.0694$ for 509 $F_o > 4\sigma(F)$ reflections. The 2*H* polytype has space group $P6_3$ and cell parameters $a = 4.83380(17)$, $c = 16.4362(9)$ Å, $V = 332.59(2)$ Å^3 and $Z = 2$ and the 3*R* polytype has space group *R*-3 and cell parameters $a = 4.835(2)$, $c = 24.496(15)$ Å, $V = 495.9(5)$ Å^3 and $Z = 3$. The sabieite polytypes (including the original sabieite from Sabie, South Africa, which is the 1*T* polytype) have glaserite-like structures with layers consisting of $Fe^{3+}O_6$ octahedra that share each of their vertices with SO_4 tetrahedra. NH_4 groups occupy 12-coordinated sites in the interlayer region, bonding to 6 O atoms in each of the adjacent layers. In the 1*T* polytype, successive layers have identical configuration and orientation, providing a one-layer repeat sequence. In the 2*H* polytype, alternate layers are flipped (or rotated), in a two-layer repeat sequence. In the 3*R* polytype, successive layers are shifted relative to one another, in a three-layer repeat sequence. The different orientations of adjacent layers in the structures of the 2*H* and 3*R* polytypes result in significant changes in the linkages between the $(NH_4)O_{12}$ and $Fe^{3+}O_6$ polyhedra.

Keywords: sabieite; crystal structure; polytype; glaserite-like structure; Huron Shale burn site, Milan, Ohio.

INTRODUCTION

The mineral sabieite, $NH_4Fe^{3+}(SO_4)_2$, was described by Martini (1983) from the Lone Creek Fall Cave, near Sabie, Eastern Transvaal, South Africa. It was found along with two

other new minerals, lonecreekite and clairite, in a suite of secondary sulfates, most of which contained ammonium. The phases were presumed to have formed at ambient temperature from seepage water, which oxidized pyrite in the chert breccia above the cave and then interacted with ammonia vapors from decaying organic matter (Hyrax excreta). The sabieite was reportedly derived from the dehydration of lonecreekite, $NH_4Fe^{3+}(SO_4)_2 \cdot 12H_2O$.

Sabieite occurred as a white powder consisting of minute platelets no more than 10 μm in diameter and too small for single-crystal study; however, powder X-ray diffraction confirmed the mineral to be essentially identical to synthetic $NH_4Fe^{3+}(SO_4)_2$ (JCPDS #24-44), with the trigonal space group *P*321 and possessing a glaserite-like structure. Martini (1983) reported the cell parameters $a = 4.822$ and $c = 8.1696$ Å ($Z = 1$) obtained from the powder data. The only other descriptive data reported was an electron microprobe analysis that provided the empirical formula $[(NH_4)_{0.83}K_{0.04}]_{\Sigma 0.87}(Fe_{0.94}Al_{0.04})_{\Sigma 0.98}S_{2.03}O_8$.

In early 2011 a remarkable suite of minerals was discovered along the Huron River in north-central Ohio. These minerals were actively forming as the result of a fire in an oil-bearing shale. Among them were several phases that appeared to be new mineral species. One of these, occurring as well-formed hexagonal plates, possesses the same ideal formula as sabieite, but provides a unique powder X-ray diffraction pattern. Further study showed the pattern to be produced by two different $NH_4Fe^{3+}(SO_4)_2$ polytypes: a 2*H* polytype with a primitive hexagonal space group ($P6_3$) and a 2-layer repeat along *c* and a 3*R* polytype with a rhombohedral trigonal space group (*R*-3) and a 3-layer repeat along *c*. The original sabieite of Martini (1983), with a 1-layer repeat along *c*, is the 1*T* polytype. According to the rules of the Commission on New Minerals Nomenclature and Classification (see Nickel and Grice, 1998), polytypes are not regarded as separate species; thus, these three phases are designated sabieite-1*T*, sabieite-2*H* and sabieite-3*R*.

Note that staff members of the Geoscience Museum of the Council for Geoscience, South Africa were unable to confirm the presence of sabieite in the minute and quite heterogeneous sample preserved as the holotype in their collection; therefore additional studies on sabieite-1*T* were not possible. The sample used in the present study is deposited in the collections of the Natural History Museum of Los Angeles County, 900 Exposition Boulevard, Los Angeles, CA 90007, USA, catalogue number 64107.

OCCURRENCE

The crystals composed of sabieite-2*H* and sabieite-3*R* occur in a suite of minerals that resulted from a natural fire in an oil-bearing shale exposed at the interface between an eroded stream cliff (up to 7.5 m high) and its talus pile (~4.5 m thick) along the Huron River in north-central Ohio, approximately 1.5 km west of Milan, Ohio (41°16'41.4"N 82°40'27"W). The fire started in early 2010, as the result of spontaneous combustion, and burned until March of 2011 (Fig. 1). The occurrence is referred to as the Huron Shale burn site.

The rock unit exposed is the late Devonian Huron Shale member of the Ohio Shale formation, a dark grey to black marine, carbon-rich shale containing ironstone concretions, finely divided pyrite and pyrite nodules and >10% organic matter. Exploratory testing at a nearby exposure produced 5.2 gallons of oil per ton. The geometry of the talus slope favors access of oxygen to pyrite, but also the sequestration of heat, which led to the spontaneous combustion. The fire was confined to the interface between talus slope and cliff. It burned to a depth of 3 m, but did not burn over any appreciable area on the surface. The mineral suite formed by sublimation and condensation on the surfaces of rocks within the talus pile (Fig. 2). Temperatures measured in a vent in the talus slope at approximately 1 meter depth were

greater than 425°C; the crystallized phases formed as gases from the fire cooled. The cliff and talus slope formed as the result of natural erosion; the fire occurred without any form of human intervention and was sustained naturally by the oil in the shale.

Other minerals in the association include alunogen, anhydrite, gypsum, letovicite, mascagnite, metavoltine, pyracmonite, salammoniac, sulfur, tschermigite, voltaite and at least two other potentially new minerals (currently under study). Minerals directly associated with sabieite include pyracmonite, tschermigite and voltaite.

The 2*H* and 3*R* polytypes could not be separated for the determination of physical and optical properties and composition, but are expected to be essentially identical in these respects. The physical and optical properties of sabieite-1*T* are also expected to be essentially the same as those for the 2*H* and 3*R* polytypes.

APPEARANCE AND PROPERTIES

The crystals are hexagonal tablets up to about 0.5 mm in diameter and 0.05 mm thick (Fig. 3). The tablets are flattened on {001} and bounded by multiple hexagonal pyramids, resulting in striated and somewhat rounded pyramid faces. The forms observed, based upon the cell for the 2*H* polytype, are {001}, {00-1} and multiple small {0*kl*} forms. Reflecting goniometer signals are consistent with the following forms: {011}, {012}, {013}, {016} and {023} (Fig. 4). Twinning is ubiquitous by reflection on {001}.

Crystals are very nearly colorless, but may be tinted pale pink, tan or yellow. The streak is white. Crystals are transparent with vitreous luster and display no fluorescence. The Mohs hardness based upon scratch tests is 2½. Tenacity is brittle, fracture is irregular and cleavage is perfect on {001}. The density measured by floatation in an aqueous solution of

sodium polytungstate is 2.65(2) g·cm^{-3}. The density calculated based on the empirical formula using single-crystal cell data for the 2*H* polytype is 2.643 g·cm^{-3}.

Crystals are hydrophobic (resist wetting in distilled water). They are very slowly soluble in concentrated HCl (about 2 hours) and 70% HNO_3 (several hours). They are extremely slowly soluble in concentrated H_2SO_4 (several days).

The mineral is optically uniaxial (–) with indices of refraction $\omega = 1.657(3)$ and $\varepsilon = 1.621(5)$ determined in white light. No pleochroism was observed. The Gladstone-Dale compatibility index $1 - (K_P/K_C)$ is -0.005 for the empirical formula, in the range of superior compatibility, and 0.022 for the ideal formula, in the range of excellent compatibility (Mandarino 2007).

CHEMICAL COMPOSITION

Analyses of sabieite (11 analyses on three crystals ranging in diameter from 200–360 μm) were performed at the University of Utah on a Cameca SX-50 electron microprobe with four wavelength-dispersive spectrometers. Analytical conditions were 15 KeV accelerating voltage, 20 nA beam current and a beam diameter of 20 μm. Counting times were 20 seconds for each element. Raw X-ray intensities were corrected for matrix effects with a phi-rho-z algorithm (Pouchou and Pichoir 1991).

Electron microprobe analysis of low atomic number elements such as nitrogen is complicated by a low cross-section for ionization and high absorption of the soft X-rays. Nitrogen was analyzed with a 60A W/Si multilayer pseudocrystal (Cameca PC-1) that provides sufficient peak intensities and suppresses spectral interferences by higher order X-ray lines of heavier elements such as Al *K*α(IV). The standard for nitrogen was synthetic

aluminum nitride. The sabieite sample and AlN standard were coated with carbon simultaneously to provide an equal thickness of the carbon coat on each. Other standards employed were sanidine (K), albite (Na), diopside (Mg), hematite (Fe), synthetic YAG (Al) and barite (S). Analyses taken systematically from the core to rim of the largest grain indicate that the sample is homogeneous within analytical precision.

The sabieite from Ohio compares favorably with the recalculated composition of the original 1*T* polytype (Table 1), including similar amounts of minor K_2O and Al_2O_3. Our analytical values for $(NH_4)_2O$ are considerably below that predicted by the structure determination and vary over a considerable range. This may, in part, be due to loss of ammonium under vacuum and it may also indicate some substitution of H_3O^+ for NH_4^+. Unfortunately, there is insufficient material for direct determination of N or H by CHN analysis. Consequently, we have added sufficient H_2O so that $NH_4^+ + K^+ + Na^+ + H_3O^+ = 1$ in the empirical formula based on S = 2. The results are presented in Table 1. The empirical formula (based on 2 S *apfu*) is $[(NH_4)_{0.73}(H_3O)_{0.22}K_{0.04}Na_{0.01}]_{\Sigma 1.00}(Fe^{3+}_{0.95}Al_{0.02}Mg_{0.01})_{\Sigma 0.98}(SO_4)_2$. The simplified formula is $NH_4Fe^{3+}(SO_4)_2$.

X-RAY CRYSTALLOGRAPHY AND STRUCTURE DETERMINATION

Both powder and single-crystal X-ray studies were carried out using a Rigaku R-Axis Rapid II curved imaging plate microdiffractometer, with monochromatized Mo$K\alpha$ radiation. For the powder-diffraction study, a Gandolfi-like motion on the φ and ω axes was used to randomize the sample. The powder pattern is a composite of the patterns from the 2*H* and 3*R* polytypes. A whole-pattern-fitting refinement using JADE 2010 (Materials Data, Inc.) and based on the structures of both polytypes indicated the intergrowth to consist of 70% of the

2*H* polytype and 30% of the 3*R* polytype. Figure 5 shows the observed powder pattern compared with those calculated from the structures of the 2*H* and 3*R* polytypes. Observed *d* values and intensities for the composite pattern were derived by profile fitting using JADE 2010 software. Data (in Å for Mo*K*α) are given in Table 2 along with the calculated patterns for each polytype. The whole-pattern-fitting refinement for the 2*H* polytype in space group $P6_3$ provided the cell parameters $a = 4.8358(18)$, $c = 16.465(8)$ Å and $V = 333.4(3)$ Å^3 and for the 3*R* polytype in space group *R*-3 it provided $a = 4.835(2)$, $c = 24.496(15)$ Å and $V = 495.9(5)$ Å^3.

For the single-crystal X-ray study, numerous tablets were cleaved and the split fragments tested until one containing only one of the polytypes was identified. This fragment, measuring 170 x 170 x 5 μm, corresponded to the 2*H* polytype, upon which the subsequent structure determination was conducted. We were unable to separate a fragment containing only the 3*R* polytype; however, its structure corresponds to that reported by Harlow and Novak (2004) for synthetic $NH_4Fe^{3+}(SO_4)_2$. The relatively large size (in two dimensions) of the crystal of the 2*H* polytype used for the structure data collection may have contributed to the rather high R factor; however, the size was necessary in order to obtain a sufficiently large data set.

The Rigaku Crystal Clear software package was used for processing of the structure data, including the application of an empirical absorption correction. The structure was solved by direct methods using SIR2004 (Burla et al. 2005). SHELXL-97 software (Sheldrick 2008) was used, with neutral atom scattering factors, for the refinement of the structure. The data quality was only fair, resulting in some instability in the S–O distances, which on average tended to be too long. In the final refinement, soft restraints of 1.43(1) Å were applied to the S–O distances, yielding reasonable results. No clear evidence for H atom positions was seen in the difference Fourier. Details of the sample, data collection, and structure refinement are

provided in Table 3, final atom coordinates and displacement parameters in Table 4, selected bond distances in Table 5 and a bond-valence analysis in Table 6.

DISCUSSION OF THE STRUCTURE

In the glaserite structure type (Moore 1973; Nikolova and Kostov-Kytin 2013) $M\mathrm{O}_6$ octahedra share each of their vertices with $T\mathrm{O}_4$ tetrahedra and each tetrahedron shares three of its vertices with octahedra, yielding a layer of formula $M(T\mathrm{O}_4)_2$. The tetrahedra surrounding each octahedron point alternately up and down into the interlayer regions above and below the layer (Fig. 6a). In the glaserite structure type, two kinds of interlayer cation sites may be populated: a 10-coordinated site (*Y*) nestled into cavities in the layers forming bonds to 9 O atoms in that layer and one O atom in the next, and a 12-coordinated site (*X*) between the layers forming bonds to six O atoms in each of the adjacent layers. As noted by Moore (1981) and further discussed by other authors (e.g. Lazoryak 1996), in the glaserite structure type, the cations and anions form two kinds of columns along *c*: column type I containing only cation polyhedra ($M\mathrm{O}_6$ octahedra alternating and sharing faces with $X\mathrm{O}_{12}$ polyhedra) and type II containing both cations and anions ($T\mathrm{O}_4$ and $Y\mathrm{O}_{10}$). In reference to the glaserite layer depicted in Figure 6a, column type I is centered on the octahedra and column type II is centered on the tetrahedra.

All three of the sabieite polytypes have glaserite-like layers consisting of $\mathrm{Fe}^{3+}\mathrm{O}_6$ octahedra and SO_4 tetrahedra. Their geometries differ from that of "ideal" glaserite (Fig 6a). In sabieite-1*T*, which is isostructural with godovikovite, $\mathrm{NH}_4\mathrm{Al}(\mathrm{SO}_4)_2$, (Boujelben et al. 2008) and steklite, $\mathrm{KAl}(\mathrm{SO}_4)_2$, (Murashko et al. 2012), the octahedra exhibit trigonal distortion (twisting), being intermediate in geometry between an octahedron and a trigonal prism (Fig.

6b). In both sabieite-2*H* and sabieite-3*R*, the octahedra are relatively undistorted, but are rotated relative to the tetrahedra (Fig. 6c). In each of the sabieite polytypes, the result is a reduction in the space between the octahedra where the *Y* site is located in the glaserite structure. In all three sabieite polytypes, the equivalent of the 12-coordinated *X* site is fully occupied by an NH_4 group and the 10-coordinated *Y* site is vacant.

The sabieite polytypes are mainly distinguished by the stacking sequences of their layers. In the 1*T* polytype, successive layers have identical configuration and orientation, providing a one-layer repeat sequence. In the 2*H* polytype, alternate layers are flipped (or rotated), in a two-layer repeat sequence. In the 3*R* polytype, successive layers are shifted relative to one another, in a three-layer repeat sequence. The layer sequences are shown in Figure 7.

It is noteworthy that, in spite of the different stacking sequences involving different successive layer orientations, the coordination polyhedron of the NH_4 group in each polytype appears to be very nearly the same (Fig. 8). Furthermore, the interlayer spacings and packing efficiencies are about the same, as indicated by the *c* cell parameters and calculated densities, respectively (Table 7). However, careful examination of the linkages of the $(NH_4)O_{12}$ polyhedra with the surrounding structural elements reveals a crucial topological difference between the three polytypes. The $(NH_4)O_{12}$ polyhedron in the sabieite-1*T* structure shares opposite faces with $Fe^{3+}O_6$ octahedra, thereby participating in the type I cation column typical of glaserite structures. In contrast, as a result of the different orientations of adjacent layers in the sabieite-2*H* structure, the $(NH_4)O_{12}$ polyhedron shares only one face with an $Fe^{3+}O_6$ octahedron and the opposite face shares corners with three different $Fe^{3+}O_6$ octahedra. In the sabieite-3*R* structure, $(NH_4)O_{12}$ polyhedron shares no face with an $Fe^{3+}O_6$ octahedron, but rather shares both opposing faces only with corners of $Fe^{3+}O_6$ octahedra. Thus, the glaserite type I column does not exist in the structure of either sabieite-2*H* or sabieite-3*R*.

IMPLICATIONS

Phases with glaserite-type and glaserite-like structures are of significant scientific interest, and they have been extensively studied for their interesting properties, including temperature-induced phase transitions without changes in topology. As a whole, these phases are remarkable for their compositional diversity, topological versatility and formation in a wide range of conditions (Nikolova and Kostov-Kytin 2013). The discovery of well-formed crystals composed of the 2*H* and 3*R* polytypes of sabieite from a unique natural occurrence has afforded the opportunity to better characterize the species and has provided new insights into the polytypic variations possible in glaserite-related structures.

As noted above, the crystals from the Huron Shale burn site, which are mixtures of the 2*H* and 3*R* polytypes of sabieite, formed by sublimation from relatively high-temperature gases, while sabieite-1*T* from the Lone Creek Fall Cave formed by dehydration of lonecreekite at ambient temperatures. This raises the possibility that the sabieite polytypes may exhibit temperature-induced phase transitions from one to another. If so, such phase transitions would differ from those previously reported for glaserite-type structures. For example, as noted by Bregiroux et al. (2009) for BaM(PO$_4$)$_2$ (M = Ti, Zr, Hf, Sn), the transition between the low-temperature monoclinic ($C2/m$) α-structure and the high-temperature trigonal (P-3m1) β-structure involves an "unfolding" of the glaserite M(PO$_4$)$_2$ layers in which the MO$_6$ and PO$_4$ polyhedra rotate relative to one another. This unfolding serves to increase the volume of the Ba polyhedron, and at the transition, the Ba coordination increases from 10 to 12. In the low-temperature form, the Ba and M polyhedra share edges, while in the high-temperature form they share faces; however, this is not the result of a

significant shift in position of the Ba polyhedron relative to the $M(PO_4)_2$ layer, as is the case for the NH_4 polyhedra relative to $Fe^{3+}(SO_4)_2$ layers in the sabieite polytypes.

It seems very likely that polytypic relationships, similar to those for the sabieite polytypes, exist for other glaserite-related structures; however, because they have not been previously reported in studies of the thermal behavior of glaserite-type phases, it may be that they are not generally manifest as temperature-induced phase transitions.

ACKNOWLEDGEMENTS

Reviewer Joel Grice, an anonymous reviewer and the Technical Editor are thanked for their constructive comments on the manuscript. Will Shewfelt is acknowledged for bringing this mineral occurrence to the attention of the scientific community via the late Ernest Carlson of Kent State University. Ernest Carlson, Lance Kearns of John Madison University and George Robinson of the A.E. Seaman Mineralogical Museum (Michigan Technological University) are acknowledged for initial studies on the minerals from this occurrence. Ellen de Kock of the Council for Geoscience, South Africa is thanked for her efforts in locating the holotype specimen of sabieite and for providing a copy of the Martini (1983) paper. Maria Atanasova of that organization is thanked for efforts to identify sabieite on the holotype specimen by powder diffraction. The electron microprobe laboratory at the University of Utah is supported in part by the National Science Foundation, the College of Mines and Earth Sciences, and the Department of Geology and Geophysics. Wil Mace of that department is acknowledged for assistance with the microprobe analyses. A portion of this investigation was funded by the John Jago Trelawney Endowment to the Mineral Sciences Department of the Natural History Museum of Los Angeles County.

REFERENCES

Boujelben, M., Toumi, M., and Mhiri, T. (2008) X-ray structure determination of $NH_4Al(SO_4)_2$. Annales de Chimie (Paris), 33, 379–386.

Bregiroux, D., Popa, K., Jardin, R., Raison, P.E., Wallez, G., Quarton, M., Brunelli, M., Ferrero, C., and Caciuffo, R. (2009) Crystal structure and thermal expansion of the low-

and high-temperature forms of $BaM^{IV}(PO_4)_2$ compounds (M = Ti, Zr, Hf and Sn). Journal of Solid State Chemistry, **182**, 1115–1120.

Burla, M.C., Caliandro, R., Camalli, M., Carrozzini, B., Cascarano, G.L., De Caro, L., Giacovazzo, C., Polidori, G., and Spagna, R. (2005) SIR2004: an improved tool for crystal structure determination and refinement. Journal of Applied Crystallography, 38, 381–388.

Harlow, R.L. and Novak, J.M. (2004) Iron ammonium bis(sulfate) as by-product of aniline production. ICSD Private Communication, ICSD #413817.

Lazoryak, B.I. (1996) Design of inorganic compounds with tetrahedral anions. Russian Chemical Reviews, 65, 287–305.

Mandarino, J.A. (2007) The Gladstone–Dale compatibility of minerals and its use in selecting mineral species for further study. Canadian Mineralogist, 45, 1307–1324.

Martini, J. E.J. (1983) Lonecreekite, sabieite, and clairite, new secondary ammonium ferric-iron sulfates from Lone Creek Fall cave, near Sabie, eastern Transvaal. Annals of the Geological Survey (South Africa), 17, 29–34.

Moore, P.B. (1973) Bracelets and pinwheels: a topological-geometrical approach to the calcium orthosilicate and alkali sulfate structures. American Mineralogist 58, 32–42.

Moore, P.B. (1981) Complex crystal structures related to glaserite, $K_3Na(SO_4)_2$: evidence for very dense packings among oxysalts. Bulletin de la Société Française de Minéralogie et de Cristallographie, 104, 536–547.

Murashko, M.N., Pekov, I.V., Krivovichev, S.V., Chernyatyeva, A.P., Yapaskurt, V.O., Zadov, A.E., and Zelensky, M.E. (2012) Steklite, $KAl(SO_4)_2$: the find at Tolbachik volcano (Kamchatka, Russia), validation as a mineral species and crystal structure. Zapiski Rossiiskogo Mineralogicheskogo Obshchestva 141(4), 36–44.

331 Nickel, E.H. and Grice, J.D. (1998) The IMA Commission on New Minerals and Mineral
332 Names: procedures and guidelines on mineral nomenclature, 1998. Canadian
333 Mineralogist, 36, 3–16.
334 Nikolova, R. and Kostov-Kytin, V. (2013) Crystal chemistry of “glaserite” type compounds.
335 Bulgarian Chemical Communications, 45, 418–426.
336 Okada, K. and Ossaka, J. (1980) Structures of potassium sodium sulphate and tripotassium
337 sodium disulphate. Acta Crystallographica, B36, 919–921.
338 Pouchou, J.-L. and Pichoir, F. (1991) Quantitative analysis of homogeneous or stratified
339 microvolumes applying the model "PAP." In: K.F.J. Heinrich and D.E. Newbury (eds)
340 Electron Probe Quantitation. Plenum Press, New York , pp. 3 l–75.
341 Sheldrick, G.M. (2008) A short history of SHELX. Acta Crystallographica, A64, 112–122.
342

FIGURE CAPTIONS

Figure 1. Huron Shale burn site along the Huron River near Milan, Ohio in early 2011.

Figure 2. Recently-formed minerals near the interface between the cliff face and talus slope. The white dendritic crystals are salammoniac. (FOV = 22 cm)

Figure 3. Hexagonal tablet of sabieite-2*H*/sabieite-3*R* with pyracmonite needles. (FOV = 0.87 mm)

Figure 4. Crystal drawing of sabieite twin (clinographic projection in standard orientation). Indexing is based upon the sabieite-2*H* cell. Note that the 0*kl* faces in the lower half of the drawing are reproduced by the {001} twin plane.

Figure 5. Observed (obs) powder diffraction pattern of sabieite crystals from Milan, Ohio compared with those simulated from the structures of sabieite-2*H* and sabieite-3*R*.

Figure 6. Polyhedral sheets viewed down [001] in (a) glaserite (aphthitalite; Okada and Ossaka 1980), (b) sabieite-1*T* (based on steklite; Murashko et al. 2012) and (c) sabieite-2*H*. Views are down [001]. Unit cells are shown by dashed lines. [Note that the atom positions for steklite provided by Murashko et al. (2012) are in error (Sergey Krivovichev, pers. comm.); for the S and O1 sites, the x coordinates given as 3/4 should be 2/3.]

Figure 7. Atomic arrangements of sabieite-1*T*, -2*H* and -3*R*, viewed with [001] approximately vertical. Unit cells are outlined.

Figure 8. NH_4 coordinations in sabieite-1*T*, -2*H* and -3*R*, viewed with [001] approximately vertical. N atoms of NH_4^+ groups are shown as dark gray spheres (red online). O atoms are shown as white spheres. NH_4^+–O bonds are shown as sticks. Edges of coordination polyhedra are shown as thin lines with thicker lines indicating faces shared with $Fe^{3+}O_6$ octahedra.

370 Table 1. Analytical results for sabieite.
371

Oxide	wt%	SD	Norm. wt%	Holotype**	$(NH_4)Fe(SO_4)_2$
$(NH_4)_2O$	6.83	0.57	7.21	8.18	9.79
K_2O	0.68	0.13	0.72	0.70	-
Na_2O	0.07	0.02	0.07	-	-
MgO	0.17	0.08	0.19	-	-
Fe_2O_3	27.27	0.63	28.78	28.64	30.02
Al_2O_3	0.28	0.29	0.30	0.68	-
SO_3	57.33	0.94	60.50	61.80	60.19
H_2O*	2.12		2.24	-	
Total	94.76		100	100.00	100

372 * Based on the structure, assuming $NH_4^+ + K^+ + Na^+ + H_3O^+ = 1$.
373 ** Lone Creek Fall Cave, S. Africa; recalculated after deducting 12.77% insoluble in HCl
374 (Martini 1983).
375

Table 2. Powder X-ray diffraction data for sabieite.

		sabieite-2*H*			sabieite-3*R*		
I_{obs}	d_{obs}	d_{calc}	I_{calc}	*h k l*	d_{calc}	I_{calc}	*h k l*
100	8.228(19)	8.2332	70	0 0 2	8.1661	23	0 0 3
14	4.102(15)	4.1880	1	1 0 0	4.1272	4	1 0 1
		4.0588	8	1 0 1	3.9620	2	0 1 2
64	3.733(5)	3.7328	43	1 0 2			
62	3.453(6)				3.4565	30	1 0 4
28	3.328(6)	3.3295	34	1 0 3			
					3.1831	1	0 1 5
10	2.938(7)	2.9358	10	1 0 4			
6	2.717(14)	2.7444	2	0 0 6	2.7220	1	0 0 9
					2.6853	2	1 0 7
7	2.587(6)	2.5887	10	1 0 5			
					2.4718	3	0 1 8
39	2.419(2)	2.4179	15	1 1 0	2.4174	6	1 1 0
		2.3923	2	1 1 1			
9	2.316(5)	2.2954	2	1 0 6	2.3180	2	1 1 3
3	2.213(12)	2.2127	7	1 1 3			
					2.1145	1	1 0 10
15	2.082(7)	2.0849	1	1 1 4	2.0802	3	1 1 6
		2.0773	1	2 0 1			
4	2.039(13)	2.0510	5	1 0 7			
		2.0294	2	2 0 2	1.9810	2	0 2 4
22	1.959(5)	1.9565	6	2 0 3	1.9663	2	0 1 11
		1.9490	2	1 1 5	1.9252	1	2 0 5
8	1.860(9)	1.8664	2	2 0 4			
		1.8473	3	1 0 8			
6	1.811(6)	1.8142	2	1 1 6	1.8075	1	1 1 9
3	1.765(6)	1.7670	4	2 0 5			
2	1.725(8)				1.7283	2	2 0 8
3	1.661(13)	1.6766	1	1 0 9			
		1.6647	1	2 0 6			
		1.6466	1	0 0 10	1.6332	1	0 0 15
					1.6145	1	0 1 14
25	1.563(2)	1.5756	2	2 1 1	1.5793	1	1 2-1
		1.5673	5	1 1 8			
		1.5641	2	2 0 7			
		1.5544	3	2 1 2	1.5597	2	1 1 -12
14	1.524(2)				1.5322	3	1 2-4
		1.5209	5	2 1 3	1.5254	1	2 0 11
3	1.476(6)	1.4774	2	1 2 4			
		1.4679	1	2 0 8			
		1.4590	1	1 1 9	1.4420	1	2 1 7
2	1.428(5)	1.4267	3	1 2 5			
21	1.3957(11)	1.4096	1	1 0 11	1.4059	1	2 1-8
		1.3960	6	3 0 0	1.3957	2	3 0 0
		1.3764	2	3 0 2	1.3757	1	0 3 3
		1.3722	1	0 0 12			
		1.3712	1	1 2 6			
18	1.362(2)	1.3610	5	1 1 10	1.3533	2	1 1 -15

Calculated intensities have been multiplied by 0.7 for sabieite-2*H* and 0.3 for sabieite-3*R* in accord with the refined proportions of each component in the powder pattern.

Table 3. Sample and crystal data for sabieite-2*H*.

Diffractometer	Rigaku R-Axis Rapid II
X-ray radiation/power	Mo$K\alpha$ (λ = 0.71075 Å)/50 kV, 40 mA
Temperature	298(2) K
Structural Formula	$NH_4Fe^{3+}(SO_4)_2$
Space group	$P6_3$
Unit cell dimensions	a = 4.83380(17) Å
	c = 16.4362(9) Å
V	332.59(2) Å^3
Z	2
Density (for above formula)	2.656 g·cm^{-3}
Absorption coefficient	2.908 mm^{-1}
F(000)	266
Crystal size	170 x 170 x 5 μm
θ range	2.48 to 27.37°
Index ranges	$-6 \le h \le 6$, $-6 \le k \le 6$, $-21 \le l \le 21$
Refls collected / unique	7037 / 513; R_{int} = 0.052
Reflections with $F_o > 4\sigma(F)$	509
Completeness to θ = 27.37°	98.6%
Max. and min. transmission	0.9856 and 0.6377
Refinement method	Full-matrix least-squares on F^2
Parameters refined	38
GoF	1.097
Final R indices [$F_o > 4\sigma(F)$]	R_1 = 0.0694, wR_2 = 0.1892
R indices (all data)	R_1 = 0.0696, wR_2 = 0.1894
Absolute structure parameter	0.13(13)
Largest diff. peak / hole	+1.99 / –1.10 e/A^3

*$R_{int} = \Sigma|F_o^2\text{-}F_o^2(\text{mean})|/\Sigma[F_o^2]$. GoF = $S = \{\Sigma[w(F_o^2-F_c^2)^2]/(n-p)\}^{1/2}$. $R_1 = \Sigma||F_o|\text{-}|F_c||/\Sigma|F_o|$. $wR_2 = \{\Sigma[w(F_o^2-F_c^2)^2]/\Sigma[w(F_o^2)^2]\}^{1/2}$; $w = 1/[\sigma^2(F_o^2) + (aP)^2 + bP]$ where a is 0.1104, b is 4.7986 and P is $[2F_c^2 + \text{Max}(F_o^2,0)]/3$.

Table 4. Atom coordinates and displacement parameters (Å^2) for sabieite-2*H*.

	x/*a*	*y*/*b*	*z*/*c*	U_{eq}	U_{11}	U_{22}	U_{33}	U_{23}	U_{13}	U_{12}
NH4	0.3333	0.6667	0.1478(17)	0.023(5)	0.019(6)	0.019(6)	0.031(13)	0.000	0.000	0.009(3)
Fe	0.6667	0.3333	-0.0980(3)	0.0120(8)	0.0094(10)	0.0094(10)	0.0173(14)	0.000	0.000	0.0047(5)
S1	0.0000	0.0000	0.0035(3)	0.0128(11)	0.0116(15)	0.0116(15)	0.015(2)	0.000	0.000	0.0058(7)
S2	0.6667	0.3333	0.2990(3)	0.0091(12	0.0070(16)	0.0070(16)	0.013(3)	0.000	0.000	0.0035(8)
O1	0.0000	0.0000	0.0910(7)	0.031(5)	0.042(7)	0.042(7)	0.009(9)	0.000	0.000	0.021(4)
O2	0.303(2)	0.277(2)	-0.0252(8)	0.027(2)	0.029(6)	0.038(6)	0.016(5)	0.003(6)	0.003(5)	0.019(5)
O3	0.6667	0.3333	0.2109(7)	0.015(4)	0.016(6)	0.016(6)	0.013(9)	0.000	0.000	0.008(3)
O4	0.622(3)	0.024(2)	0.3305(9)	0.029(3)	0.025(6)	0.019(5)	0.039(7)	-0.005(5)	-0.003(6)	0.009(4)

Table 5. Selected bond distances (Å) for sabieite-2*H*.

NH_4–O1 (×3)	2.943(10)	Fe–O4 (×3)	1.975(12)	S1–O1	1.438(11)	S2–O3	1.447 (11)
NH_4–O3 (×3)	2.977(10)	Fe–O2 (×3)	2.027(12)	S1–O2 (×3)	1.483(9)	S2–O4 (×3)	1.493(10)
NH_4–O2 (×3)	3.37 (3)	<Fe–O>	2.006	<S1–O>	1.472	<S2–O>	1.482
NH_4–O4 (×3)	3.40(3)						
<NH_4–O>	3.173						

Table 6. Bond-valence analysis for sabieite-2*H*. Values are expressed in valence units.

	O1	O2	O3	O4	Σ_c
NH_4	0.14 ×3↓→	0.04 ×3→	0.13 ×3↓→	0.04 ×3→	1.05
Fe		0.48 ×3→		0.56 ×3→	3.12
S1	1.65	1.46 ×3→			6.03
S2			1.61	1.42 ×3→	5.87
Σ_a	2.07	1.98	2.00	2.02	

Multiplicities indicated by ×↓→; NH_4^+–O and Fe^{3+}–O bond strengths from Brown and Altermatt (1985); Si^{4+}–O bond strengths from Brese and O'Keeffe (1991).

Table 7. Comparison of unit cells of the sabieite polytypes.

	Sabieite-1*T**	Sabieite-2*H*†	Sabieite-3*R*‡
Space group	*P*321	$P6_3$	*R*-3
a (Å)	4.822	4.83380(17)	4.835(2)
c (Å)	8.1696	16.4362(9)	24.496(15)
V (Å^3)	164.51	332.59(2)	495.9(5)
Z	1	2	3
Density (g·cm^{-3})§	2.685	2.656	2.672

* Martini (1983)
† Refined from single-crystal data.
‡ Refined from powder data.
§ For ideal composition.

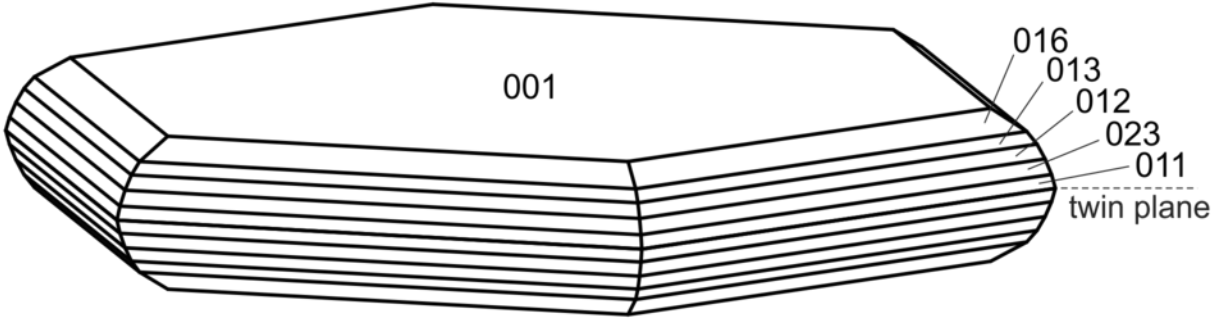
001
016
013
012
023
011
twin plane

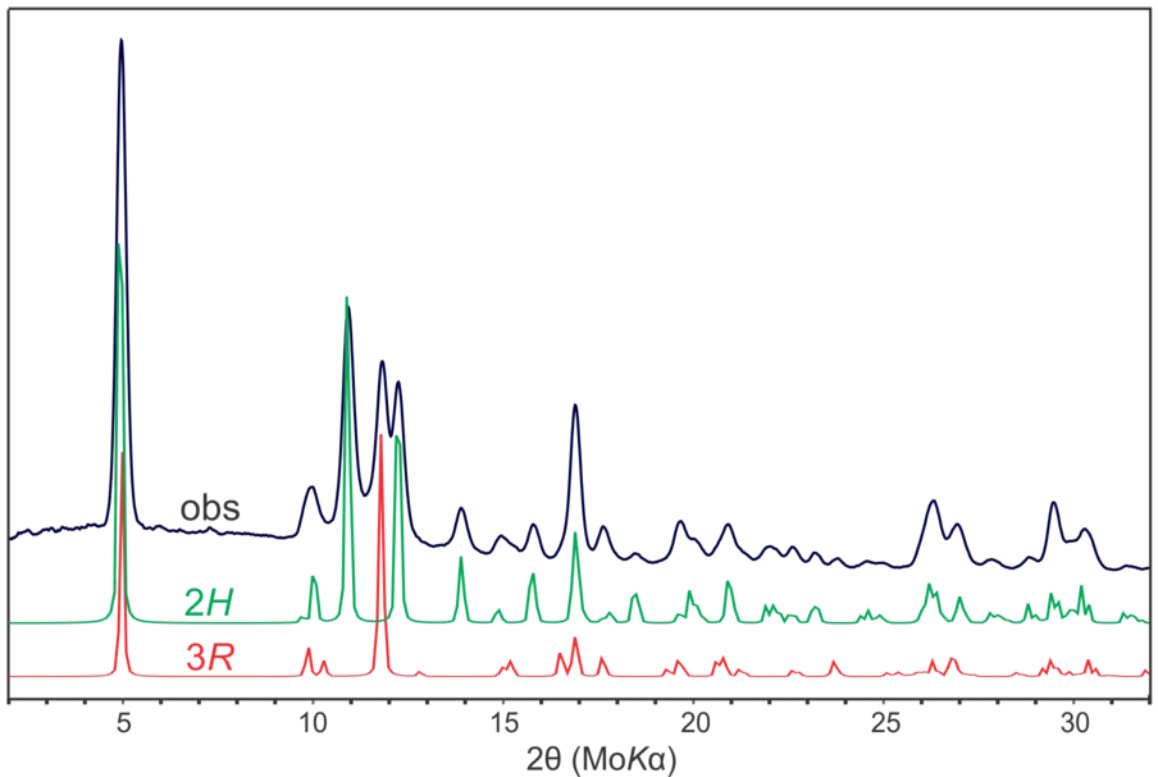
obs
2H
3R
5
10
15
20
25
30
2θ (MoKα)

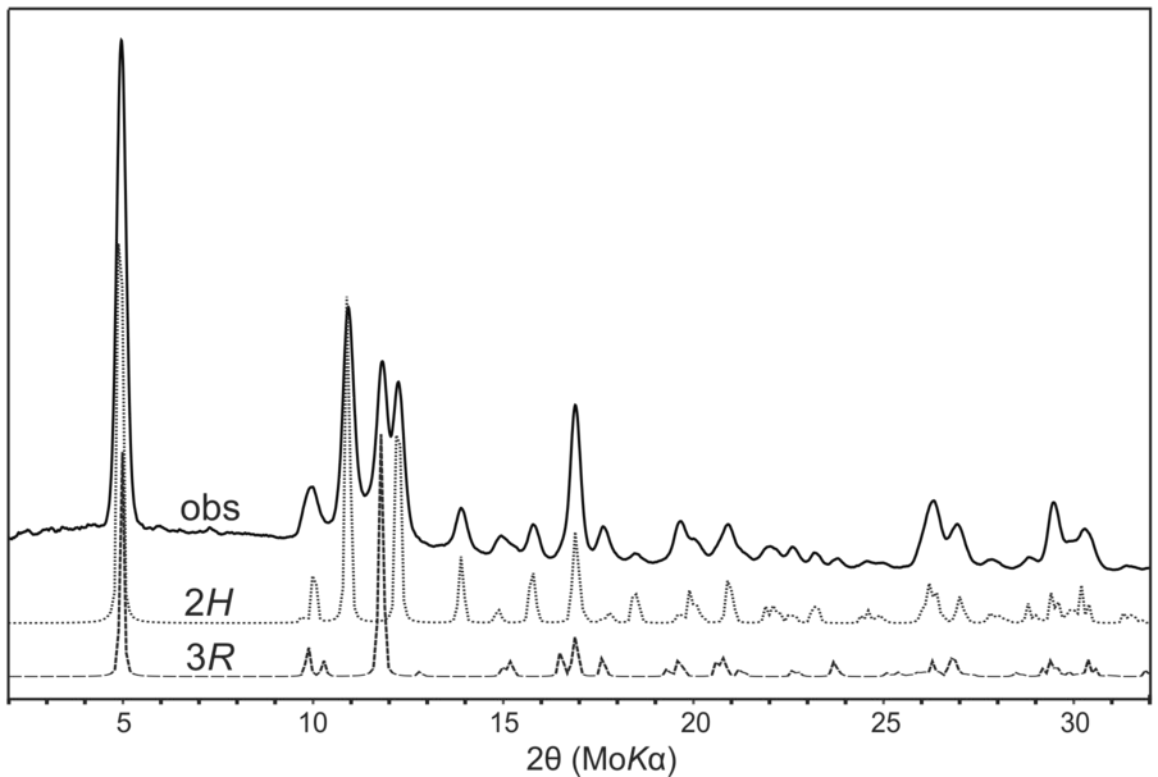
obs
2H
3R
5
10
15
20
25
30
2θ (MoKα)

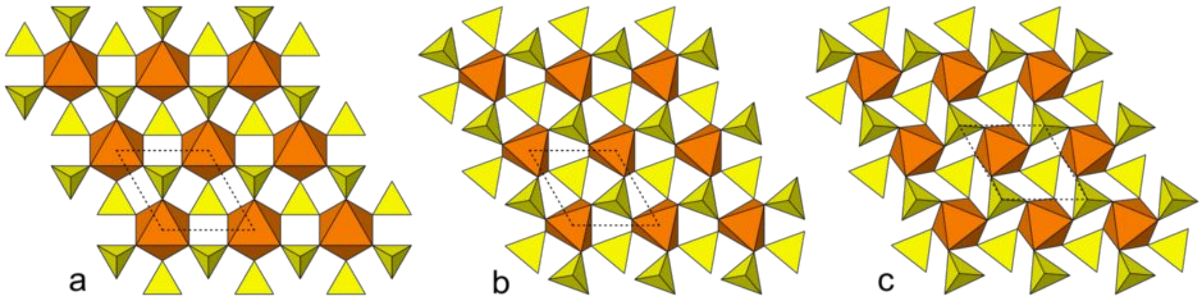
a
b
c

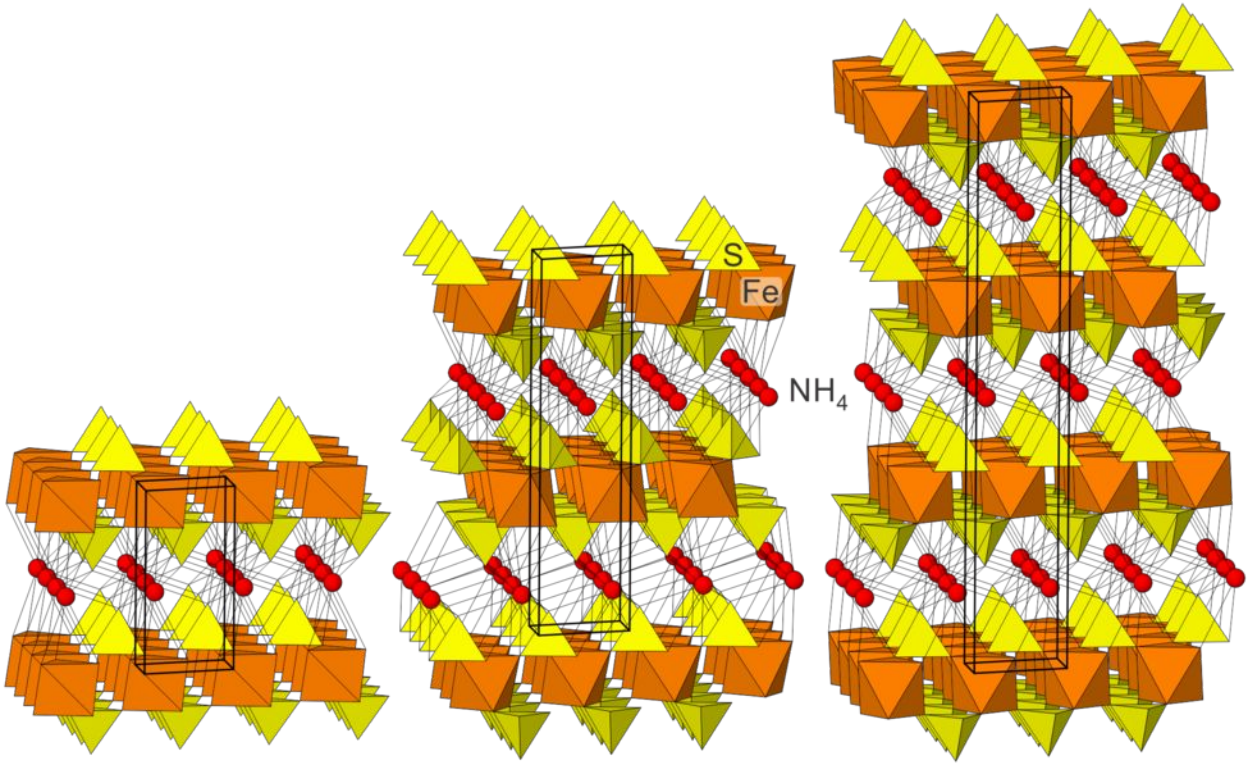
S
Fe
NH4
sabieite-1T
sabieite-2H
sabieite-3R

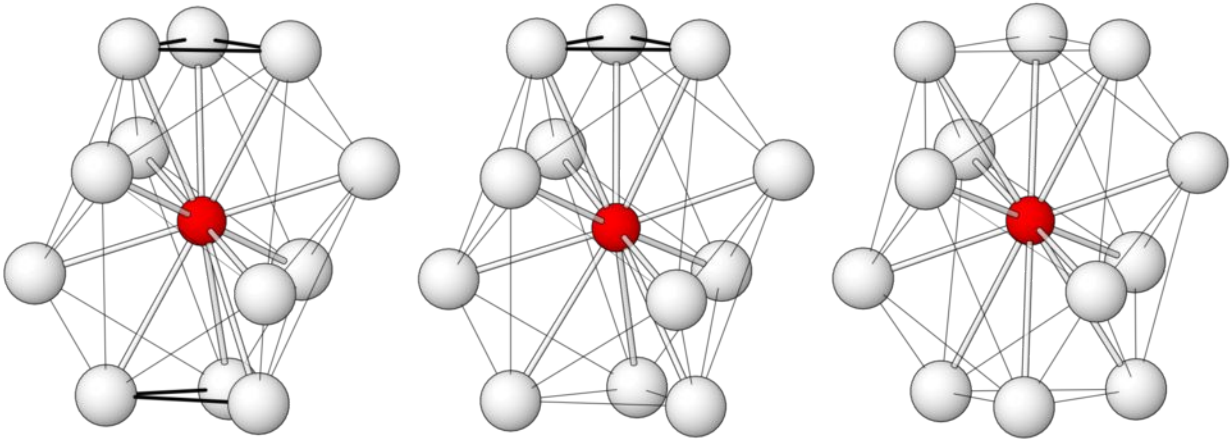
1T
2H
3R